Acta Crystallographica Section D
Biological Crystallography
ISSN 0907-4449

Structure of rabbit liver fructose 1,6-bisphosphatase at 2.3 Å resolution

Charles M. Weeks,[a] Aleksander W. Roszak,[a]† Mary Erman,[a] Rudolf Kaiser,[b] Hans Jörnvall[b] and Debashis Ghosh[a,c]*

[a]Hauptman–Woodward Medical Research Institute, 73 High Street, Buffalo, NY 14203-1196, USA, [b]Department of Medical Biochemistry and Biophysics, Karolinska Institutet, S-171 77, Stockholm, Sweden, and [c]Roswell Park Cancer Institute, Elm and Carlton Streets, Buffalo, NY 14263, USA

† Present address: Department of Chemistry, University of Glasgow, Glasgow G12 8QQ, Scotland.

Correspondence e-mail: ghosh@hwi.buffalo.edu

Received 23 March 1998
Accepted 24 June 1998

PDB Reference: fructose 1,6-bisphosphatase, 1bk4.

The three-dimensional structure of the R form of rabbit liver fructose 1,6-bisphosphatase (Fru-1,6-Pase; E.C. 3.1.3.11) has been determined by a combination of heavy-atom and molecular-replacement methods. A model, which includes 2394 protein atoms and 86 water molecules, has been refined at 2.3 Å resolution to a crystallographic *R* factor of 0.177. The root-mean-square deviations of bond distances and angles from standard geometry are 0.012 Å and 1.7°, respectively. This structural result, in conjunction with recently redetermined amino-acid sequence data, unequivocally establishes that the rabbit liver enzyme is not an aberrant bisphosphatase as once believed, but is indeed homologous to other Fru-1,6-Pases. The root-mean-square deviation of the Cα atoms in the rabbit liver structure from the homologous atoms in the pig kidney structure complexed with the product, fructose 6-phosphate, is 0.7 Å. Fru-1,6-Pases are homotetramers, and the rabbit liver protein crystallizes in space group *I*222 with one monomer in the asymmetric unit. The structure contains a single endogenous Mg^{2+} ion coordinated by Glu97, Asp118, Asp121 and Glu280 at the site designated metal site 1 in pig kidney Fru-1,6-Pase R-form complexes. In addition, two sulfate ions, which are found at the positions normally occupied by the 6-phosphate group of the substrate, as well as the phosphate of the allosteric inhibitor AMP appear to provide stability. Met177, which has hydrophobic contacts with the adenine moiety of AMP in pig kidney T-form complexes, is replaced by glycine. Binding of a non-hydrolyzable substrate analog, β-methyl-fructose 1,6-bisphosphate, at the catalytic site is also examined.

1. Introduction

Fructose 1,6-bisphosphatase (Fru-1,6-Pase; D-fructose 1,6-bisphosphate 1-phosphohydrolase; E.C. 3.1.3.11) catalyzes the hydrolysis of the α anomer of fructose 1,6-bisphosphate to α-D-fructose 6-phosphate and inorganic phosphate (Benkovic & deMaine, 1982). It was first described by Gomori (1943) who separated it from other phosphatases present in mammalian tissues. Fru-1,6-Pase is involved in several metabolic pathways. In mammalian liver and kidney, it catalyzes a key regulatory step in gluconeogenesis (Marcus, 1981; Van Schaftingen & Hers, 1981; Benkovic & deMaine, 1982; Tejwani, 1983; Van Schaftingen, 1987), and it also serves a gluconeogenic function in yeasts and in *Escherichia coli*, where it is necessary for growth on substances such as glycerol and succinate. In eukaryotic plants, a gluconeogenic Fru-1,6-Pase found in the cytosol takes part in sucrose synthesis from triose phosphates, while an isozyme within the chloroplasts is necessary for

regeneration of ribulose bisphosphate in the pentose phosphate pathway or Calvin cycle leading to photosynthetic carbon dioxide assimilation. This enzyme also functions in the Calvin cycle in photosynthetic and chemoautotrophic bacteria.

Active forms of mammalian Fru-1,6-Pase are homotetramers with subunit sizes of about 36 kDa (Tashima *et al.*, 1972) and maximal activity either under alkaline conditions or near physiological (neutral) pH (Traniello *et al.*, 1971). The alkaline form is the result of hydrolysis by lysosomal proteases during the isolation procedure (Pontremoli *et al.*, 1973, 1974), and this hydrolysis can be mimicked by subtilisin digestion (Horecker *et al.*, 1980). Intact neutral subunits can be cleaved at four sites in the region between residues 57 and 67, resulting in a shift of the optimum pH from 7.5 to 9.2 (Traniello *et al.*, 1972). Evolutionary conservation of this protease-sensitive region suggests a physiological role (MacGregor *et al.*, 1982). Although the significance of protease sensitivity is still unclear, other aspects of Fru-1,6-Pase regulation are well documented. A divalent metal ion such as Mg^{2+}, Mn^{2+} or Zn^{2+} is essential for activity (Gomori, 1943), and catalysis requires the formation of an enzyme–metal–substrate complex (Benkovic & deMaine, 1982). Although monovalent cations such as K^+, NH_4^+ or Tl^+ are not required, their presence is needed for maximal activity (Hubert *et al.*, 1970). The enzyme is inhibited by noncompetitive AMP interaction with an allosteric site (Taketa & Pogell, 1965; Liu & Fromm, 1990) and by D-fructose 2,6-bisphosphate (Fru-2,6-P_2) competition for the active site (Van Shaftingen & Hers, 1980).

Although the first partial sequences for rabbit liver Fru-1,6-Pase were determined some time ago (Botelho *et al.*, 1977; Suda *et al.*, 1982; Xu *et al.*, 1982), the complete amino-acid sequence of this 337-residue protein was determined only recently (Kaiser *et al.*, 1996). Based on the earlier sequences, the rabbit liver protein appeared to differ from other vertebrate forms, including those of pig kidney (Marcus *et al.*, 1982; Harrsch *et al.*, 1985; Williams & Kantrowitz, 1992), sheep liver (Fisher & Thompson, 1983), rat liver (El-Maghrabi *et al.*, 1988) and human and chicken liver (El-Maghrabi *et al.*, 1993), to a greater degree than would be expected from the homology between these other forms. The recent complete sequence determination, however, showed that the extent of residue identity with the other vertebrate enzymes is high (85–91%) and that the rabbit liver enzyme is unique at only nine positions. As expected, residue identity is lower towards plant and yeast Fru-1,6-Pases (44–57%) and also towards the enzyme of prokaryotic forms (30–43%).

Pig kidney Fru-1,6-Pase has been the subject of intense crystallographic study. R-form structures include the native apoprotein (Protein Data Bank code 2FBP; Ke *et al.*, 1989; Ke, Thorpe *et al.*, 1990) and complexes with the product Fru-6-P (5FBP; Ke, Zhang *et al.*, 1991), the competitive inhibitor Fru-2,6-P_2 (3FBP; Liang *et al.*, 1992), the substrate Fru-1,6-P_2 (1FBH; Zhang *et al.*, 1993), the α-substrate analog AhG-1,6-P_2 plus Mg^{2+} (1FBC), Mn^{2+} (1FBD) or Zn^{2+} (1FBE; Zhang *et al.*, 1993), the β-substrate analog AhM-1,6-P_2 plus Mg^{2+} (1FBF) or Mn^{2+} (1FBG; Zhang *et al.*, 1993) and Tl^+ ions (1FPK; Villeret, Huang, Fromm *et al.*, 1995). T-form complexes with the allosteric inhibitor AMP include the binary complex (4FBP; Ke, Liang *et al.*, 1991) and quaternary or higher complexes with the product Fru-6-P plus Mg^{2+} (1FBP; Ke, Zhang *et al.*, 1990), the competitive inhibitor Fru-2,6-P_2 plus Zn^{2+} (1FRP; Xue *et al.*, 1994), the α-substrate analog AhG-1,6-P_2 plus several different concentrations of Mn^{2+} (1FPD, 1FDE, 1FDF, 1FDG; Villeret, Huang, Zhang & Lipscomb, 1995) or AhG-1,6-P_2 plus the monovalent cations K^+ (1FPI), Li^+ and Tl^+ (1FPJ) or Tl^+ (1FPL; Villeret, Huang, Fromm *et al.*, 1995). Comparative analyses of these R- and T-state structures have led to the development of theories for the mechanism of the allosteric transition (Zhang *et al.*, 1994). The structures of several pig kidney mutant enzymes have also been determined. These structures include the T form of the Lys42→Ala mutant (1FSA; Lu *et al.*, 1996) and both the R form (1RDX) and T forms (1RDY and 1RDZ) of the Arg243→Ala mutant (Stec *et al.*, 1996). Crystal structures have also been reported for the enzymes from human liver (1FTA; Gidh-Jain *et al.*, 1994) and spinach chloroplast (1SPI; Villeret, Huang, Zhang, Xue *et al.*, 1995).

Although the crystallographic study of rabbit liver Fru-1,6-Pase was initiated two decades ago (McPherson *et al.*, 1977; Soloway & McPherson, 1978) and a tentative model was proposed (Weeks *et al.*, 1988), inconsistencies between the early sequence data of the rabbit liver enzyme and the electron-density maps prevented complete interpretations for many years. Only after the complete sequence became available could the ambiguities in map interpretation be resolved with confidence. The R-state crystal structure of neutral rabbit liver Fru-1,6-Pase is reported here at 2.3 Å resolution. This structure has as ligands not only an endogenous Mg^{2+} ion, but also sulfate ions at the positions normally occupied by phosphate in both the catalytic and allosteric sites.

2. Materials and methods

2.1. Enzyme purification and crystallization

Fru-1,6-Pase was purified from fresh rabbit livers (Ulm *et al.*, 1975) and activity was assayed at pH 7.5 and 9.2 to verify that the protein had not undergone partial proteolysis. Freshly isolated protein was concentrated by ammonium sulfate precipitation and washed thoroughly in Amicon stirred cells (over YM-10 membranes) with 25 m*M* Tris buffer in such a manner that any residual salt was diluted at least 10000-fold. Crystallization by the vapor-diffusion method was performed in sandwich boxes using nine-well glass plates. Reservoirs containing 10–15% PEG 4000 solutions in 25 m*M* Tris buffer (pH 7.4) were equilibrated at ambient temperature against droplets containing mixtures of 10 µl protein solution at a concentration of 7–8 mg ml^{-1}, 10 µl reservoir and 2 ml of 50–200 m*M* ammonium sulfate. Crystals, typically 0.3 × 0.4 × 2.0 mm in size, appeared in 10–14 d. The addition of appropriate concentrations of ammonium sulfate to crystallization droplets was essential for the routine growth of diffraction-quality crystals, and the careful washing of precipitated protein was necessary for reproducible results. The space group was determined to be *I*222 with unit-cell dimensions of

Table 1
Summary of data collection for native and derivative crystals.

Crystal type	$K_3UO_2F_5$ derivative	$KAu(CN)_2$ derivative	$K_3UO_2F_5$ derivative	Native	Mg β-methyl Fru-1,6-P_2 complex
Soaking conditions; number of sites	1 m*M*, 3 d; 2 major, 4 minor	—	2 m*M*, 5 d; 2 major, 4 minor	—	Co-crystallized; 1 m*M* β-methyl Fru-1,6-P_2, 1 m*M* $MgCl_2$; 1 site
Machine used	Nonius CAD4 diffractometer	Nonius CAD4 diffractometer	Siemens area detector, Argonne	UCSD multiwire Mark III	Nonius AD4 diffractometer
Number of crystals used	4	7	1	1	1
Maximum resolution (Å)	4.00	3.75	3.07	2.20	4.0
Total data	11298	11368	20100	67887	3771
Unique data	3536	4052	6367	16921	2986
Friedel pairs	Yes	Yes	Yes	No	No
$I/\sigma(I)$ overall	—	—	22.0	12.8	—
Completeness (%)	—	—	83.5	93	~95
$R(I)$ merge (%)	8.38	6.78	7.98	5.68	2.31
$R(F)$ native-to-derivative (%)	15.2	10.9	15.0	—	10.6

a = 73.79, b = 80.05 and c = 131.82 Å. The crystallographic asymmetric unit contains a single polypeptide chain (monomer or subunit) of 337 residues. Isomorphous heavy-atom derivative crystals were prepared by addition of 1–2 µl of solutions containing heavy-atom compounds to droplets with native crystals and soaking for 2–7 d.

2.2. Data collection

X-ray diffraction data sets for native and heavy-atom derivative crystals were collected over a period of several years at three facilities: (i) an in-house single-channel Nonius CAD4 diffractometer with a sealed-tube Cu anode, (ii) a Siemens area detector with a rotating anode at the Midwest Crystallography Resource in the laboratory of Dr Edwin Westbrook at Argonne National Laboratory and (iii) a Mark III multiwire detector at the Resource for Crystallography located in the laboratory of Professor Nguyen Huu Xuong at the University of California, San Diego. All data were collected using Cu $K\alpha$ radiation. The best native data set (2.30 Å resolution) was collected from one crystal on the Mark III detector. This data set was used to calculate all native electron-density maps and for the final refinement of the model. The derivative data sets were collected with the CAD4 and Siemens detectors. A summary of data-collection experiments is provided in Table 1.

2.3. Structure solution and refinement

All computations necessary for structure solution, model building and refinement were carried out on a Silicon Graphics Indigo R4000 Workstation. An initial electron-density map of the molecule was constructed by the multiple isomorphous replacement method. Heavy-atom binding sites were determined by the *HASSP* routine and refined by *HEAVY* using the origin-removed Patterson technique (Terwilliger & Eisenberg, 1983). Minor binding sites were located by double-difference Fouriers. Origin correlation between the $K_3UO_2F_5$ and $KAu(CN)_2$ derivatives, as well as independent confirmation of the heavy-atom binding sites, came from the cross-difference Fourier synthesis. The *PHASES* software package (Furey & Swaminathan, 1990) was used to combine the phase information from the isomorphous and anomalous intensity data for both derivatives, to apply solvent flattening, to calculate final combined phases and to prepare an *MIRAS*-phased Fourier synthesis at 3.5 Å resolution. Details of the phasing statistics are provided in Table 2. The protein–solvent boundary was clearly visible from this electron-density map, and many α-helices and β-sheets were interpretable. However, other regions of the density, in particular loops and turns, were poorly defined. At this time, the coordinates of the R form of pig kidney Fru-1,6-Pase (PDB code 2FBP; Ke *et al.*, 1989) became available and a molecular-replacement solution was obtained using the program *X-PLOR* (Brünger, 1992) and the 2FBP coordinates as the search model. This solution was further optimized manually by building an atomic model for the rabbit liver Fru-1,6-Pase molecule into the *ab initio* electron-density map while using the molecular-replacement solution as a guide. The program *CHAIN* (Sack, 1988) was used for this purpose. When the complete revised rabbit-liver Fru-1,6-Pase sequence data became available (Kaiser *et al.*, 1996), it was used to build the side chains into this density map. Structure factors calculated from the partially completed model were combined with the starting experimental phases using the *PHASES* package, and new electron-density maps were calculated in order to build through the regions of the molecule having poorly defined electron density or strong search-model bias. This process was continued until it was possible to account for the entire electron density in the asymmetric unit. No density could be located for the N-terminal residues Ala1–Pro5 or for the polypeptide segment corresponding to residues 54–71 (protease-sensitive area). Consequently, these regions were left out of the model, although it is clear from the sequence data (Kaiser *et al.*, 1996) that these residues are present in the polypeptide chain. The same regions also exhibit disorder in the crystal structures of the pig kidney enzyme.

Table 2
Phasing statistics and figures of merit.

(*a*) Phasing statistics from the combination of individual isomorphous derivative phases

Derivative	Reflections phased	Highest resolution (Å)	*R* factor†	Phasing power‡	Phasing power‡ in the last shell
$K_3UO_2F_5$ (CAD)	3298	4.0	0.59	2.09	1.91
(anomalous)	2272	4.0	0.43	1.64	1.10
$K_3UO_2F_5$ (MAD)	4516	3.5	0.63	2.19	2.14
(anomalous)	3387	3.5	0.45	1.74	1.34
$KAu(CN)_2$	3780	3.75	0.68	1.24	0.96
(anomalous)	2557	3.75	0.45	1.45	1.03
Methyl-Mg-Fru-biphosphate	1413	6.0	0.68	1.19	0.97

(*b*) Figure of merit (FOM) from phase combination

											Total
Mean resolution (Å)	12.20	7.00	5.81	5.16	4.72	4.40	4.15	3.95	3.76	3.59	
Number of reflections	476	476	476	476	476	476	476	476	476	476	4763
FOM	0.86	0.77	0.71	0.71	0.72	0.68	0.66	0.58	0.51	0.48	0.67

† *R* factor is $R_{\rm Cullis}$ for Friedel pair averaged data and is defined as $R = (\sum \big|\,|F_{\rm PH}| \pm |F_{\rm P}| - |f_{\rm H}|\,\big|) / (\sum |F_{\rm PH}| \pm |F_{\rm P}|)$, where P and H refer to parent and heavy-atom derivative data sets, respectively: $|F|$ measured structure amplitudes. *R* factor for anomalous data is defined as $R = \sum \big[\big||F_{\rm PH}^{\rm obs}(+)| - |F_{\rm PH}^{\rm calc}(+)|\big| + \big||F_{\rm PH}^{\rm obs}(-)| - |F_{\rm PH}^{\rm calc}(-)|\big|\big] / \sum[|F_{\rm PH}^{\rm obs}(+)| + |F_{\rm PH}^{\rm obs}(-)|]$, where + and − refer to Friedel-mate reflections. Obs: observed; Calc: calculated. ‡ Phasing power is defined as $f_{\rm H}$ r.m.s./lack of closure or $2f''_{\rm H}$(calc)/lack of closure for anomalous case.

2.4. Solvent

The complete protein model was refined with *X-PLOR*, initially at 3.0 Å resolution, using the Engh and Huber weighting scheme for geometrical restraints (Engh & Huber, 1991). After annealing, new omit maps ($2F_{\rm obs} - F_{\rm cal}$) were calculated for ambiguous regions, and these regions were then rebuilt. This process continued as the resolution of the data was gradually extended in steps to 2.3 Å. 15 cycles of simulated annealing and isotropic temperature-factor refinement, alternated with rebuilding of problem areas, yielded a bias-free protein model. The *R* factor for the 2.3 Å data with $F > 2\sigma F$ was 20.3%. The first shell of solvent water molecules, hydrogen bonded to polar surface atoms of the protein, was included in the model at this time. The positional parameters of the water O atoms were held fixed during the simulated-annealing part of the subsequent refinement and the individual thermal parameters of the water O atoms were refined isotropically. Any water oxygen that moved from the original electron density resulting in unacceptable hydrogen-bonding geometry or that exhibited a high isotropic temperature factor (>70 $Å^2$) was removed. Using these criteria, a total of 86 water molecules were included in the final model.

2.5. Ligands

A difference electron-density map computed at this time showed three distinct peaks larger than water molecules. The first such peak, which appeared to be sitting at the center of the coordinating acidic side chains of Glu97, Asp118, Asp121 and Glu280, was satisfactorily modeled as a Mg^{2+} ion. Attempts to model this density with a Mn^{2+} ion resulted in a negative residual density at that position and an isotopic temperature factor much higher than the average of the temperature factors of the neighboring atoms. Modeling as an NH_4^+ ion led to poor coordination geometry such as large distances (2.7–4.1 Å). The second difference peak, located in the vicinity of the side chains of Asn212, Tyr244, Tyr264 and Tyr215, was identified as a sulfate ion. The third difference peak, which occupied a position near the main-chain amide groups of residues Thr27, Gly28, Glu29 and Met30, as well as the side chains of Lys112 and Tyr113, was also identified as a sulfate ion. All three ions were subsequently included in the refinement and continued to exhibit acceptable hydrogen-bonding geometries as well as isotopic temperature factors consistent with those of the coordinating protein atoms. Based on the average thermal parameters, the Mg^{2+} site is fully occupied and the sulfate sites are partially occupied. Ligand occupancies were not refined.

The refinement statistics are summarized in Table 3 for the complete model consisting of protein monomer, solvent and ligands. This final model was subjected to *PROCHECK* analysis to assess its quality (Laskowski *et al.*, 1993). 88% of the 268 non-glycine and non-proline residues were in the most-favored regions of the Ramachandran plot, 12% were in additional allowed regions and none were in disallowed regions. The random positional error estimated from the Luzzati plot (Luzzati, 1952) was between 0.20 and 0.30 Å. Finally, a difference electron-density map was calculated with the 4 Å data of the β-methyl fructose-1,6-bisphosphate complex with the rabbit liver enzyme, and a molecule of this non-hydrolyzable substrate analog was manually modeled into the map by trial and error.

3. Results

3.1. Overall structure

The asymmetric unit of this crystalline form of rabbit liver Fru-1,6-Pase contained one subunit of the homotetramer, 86 water molecules, one Mg^{2+} cation and two sulfate anions. A ribbon diagram depicting this structure is shown in Fig. 1. The protein molecule is situated in the *I*222 unit cell with the center of the tetramer at the origin or intersection of three twofold axes. Consequently, the tetramer, illustrated in Fig. 2, possesses exact D_2 symmetry. The overall conformation of the monomer and the quaternary structure of the tetramer closely resemble those of the pig kidney structure (Ke *et al.*, 1989). All crystalline forms of the pig kidney enzyme examined so far have two or four subunits in the asymmetric unit, and they exhibit pseudo, rather than crystallographically exact, D_2

symmetry. The overall shape of the tetramer, consisting of subunits C1 to C4, has been described as a pseudohexagonal disk with a thickness of 35 Å.

The folding pattern of a rabbit liver subunit can be described as two-domain α/β, in agreement with previous descriptions of the three-dimensional structure of the pig kidney enzyme. The secondary structure of the subunit is summarized in Table 4. The rabbit liver protein contains three short 3_{10} helices (H5a, H5b and H8a) missing from the pig kidney structure. Domain 1, consisting of residues 1–200, is the allosteric AMP-binding domain, while residues 201–337 constitute domain 2, the catalytic domain, which is responsible for hydrolysis of the substrate. Domain 1 consists of three long α-helices (H1–H3), a β-sheet comprised of eight mixed strands (B1–B8) and two very short helical segments (H4 and H5). The β-sheet direction is parallel to the axes of the long helices. Domain 2 also has a central β-sheet with mixed strands (B9–B13). This sheet is flanked by α-helices H7 and H8 on the side towards domain 1 and by helices H6 and H9 on the side towards the exterior of the molecule. From the point of view of the orientations of the β-sheets and α-helices, the two domains are rotated by roughly 90° with respect to each other. Overall, the secondary-structure elements of the molecule are distributed in five layers, as previously described for the pig kidney apo protein (PDB code 2FBP; Ke *et al.*, 1989).

3.2. Backbone comparison to pig kidney structures

The Cα atoms of the rabbit liver subunit were fitted by least-squares to pig kidney subunits in both the R and T states. The pig kidney Fru-6-P complex (5FBP; Ke, Zhang *et al.*, 1991) having a C1C2 dimer in the asymmetric unit was chosen as the representative R-state structure and the pig kidney AMP complex (4FBP; Ke, Liang *et al.*, 1991) with a tetramer in the asymmetric unit was chosen as the representative T form. A total of 312 analogous Cα positions per monomer were used in the least-squares procedure. Table 5 summarizes the results of the fitting process in terms of root-mean-square (r.m.s.) deviations, and Fig. 3 illustrates the superposition of the rabbit liver subunit onto pig kidney R- and T-state monomers.

The r.m.s. deviations between the rabbit liver monomer and the two crystallographically independent R-state monomers of the pig kidney Fru-6-P complex are 0.69 and 0.67 Å. These

Table 3
Refinement of the apo rabbit liver fructose-1,6-bisphosphate.

Resolution range (Å)	8.0–2.23
Number of reflections used ($F > 2\sigma F$)	13678
Number of protein atoms	2394
Number of SO_4^{2-} atoms (2 ions)	10
Number of Mg^{2+} ions	1
Number of water molecules (O atoms)	86
Crystallographic R factor	0.177
R.m.s. deviations from ideal geometry	
Bonds (Å)	0.012
Angles (°)	1.7
Dihedral angles (°)	24.7
Planarity (°)	1.5
Average temperature factor (protein) (Å^2)	36.9
Ramachandran plot statistics	
Percent of 268 non-glycine and non-proline residues in the most favored region	88
Percent in the disallowed region	0

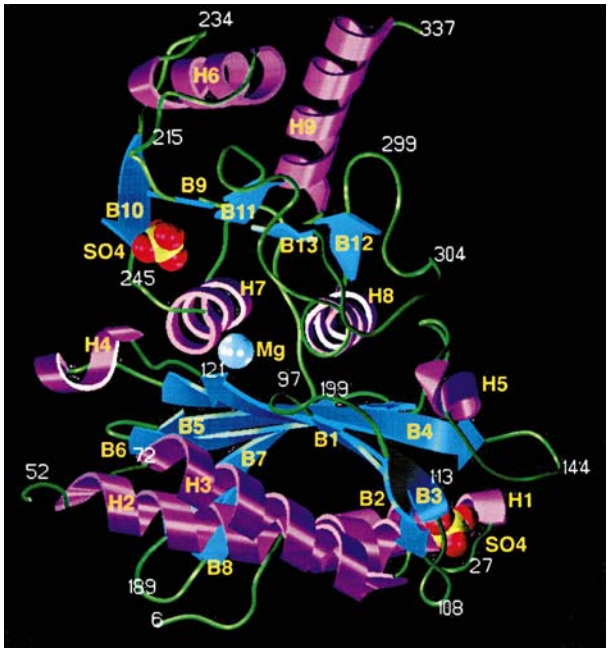

Figure 1
A ribbon diagram for the rabbit liver Fru-1,6-Pase monomer. Secondary structure elements defined in Table 4 are shown in magenta (α-helix), blue (β-strand) and green (loops). This figure was drawn using *SETOR* (Evans, 1993).

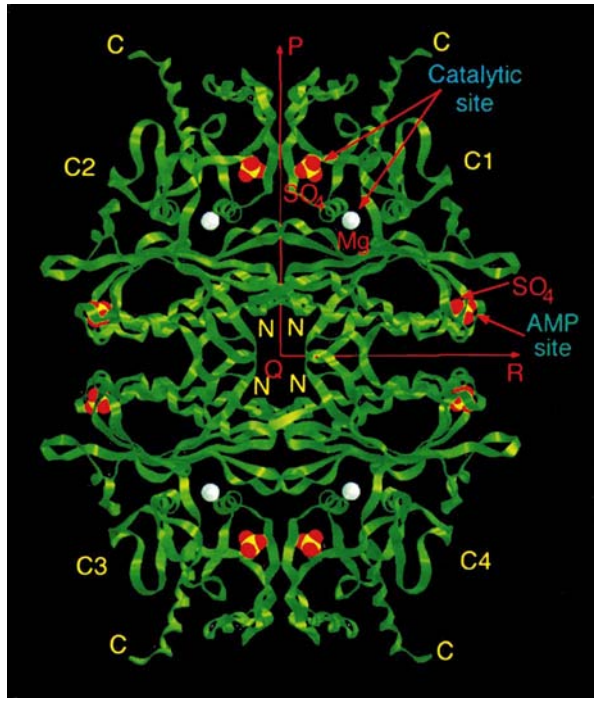

Figure 2
A ribbon diagram illustrating the D_2 symmetry of the rabbit liver Fru-1,6-Pase tetramer. The monomeric subunits are designated C1–C4. Molecular 222-symmetry axes are designated by P, Q and R. The figure was drawn using *SETOR*.

deviations are nearly twice the estimated random errors in the positional parameters of the rabbit liver structure. If only domain 1 is used in the least-squares fit, the r.m.s. deviation is 0.53 Å for domain 1 itself and 0.86 Å for domain 2, thereby indicating a small difference in relative orientation of the two domains between the rabbit liver and the R-state pig kidney structures. When the entire R-state monomers are fitted, significant deviations (>1 Å) of the Cα positions occur at (i) residues 24–26 (end of H1), (ii) residues 124–129 (H4), (iii) residues 268–271 (average deviation ∼3.6 Å; loop between B11 and H8) and (iv) the C-terminus. There are only two sequence differences between the rabbit and pig proteins in these regions (Arg25→Gly and Gln332→Lys). Conformational differences marked by backbone deviations between the two structures are, therefore, not necessarily correlated with sequence changes. Instead, the regions of the rabbit liver structure with the greatest differences consist mainly of long loops or turns which have high isotropic temperature factors for the backbone as well as for the side-chain atoms. In fact, the four regions listed above all have poor electron density (little significant density above the 1σ level) and correspond to areas with high average temperature factors (50–100 Å^2). The average isotropic thermal parameter for all backbone atoms is 36.9 Å^2, a value somewhat higher than those reported for most pig kidney structures. Comparison of the rabbit liver dimer and tetramer (generated by crystallographic symmetry) with the pig kidney R-state dimers (C1C2 or C3C4) and tetramer showed only marginal increases in the r.m.s. deviation values (0.7–0.8 Å), indicating the overall similarity not only of the monomers, but also of the R-state dimeric and tetrameric structures.

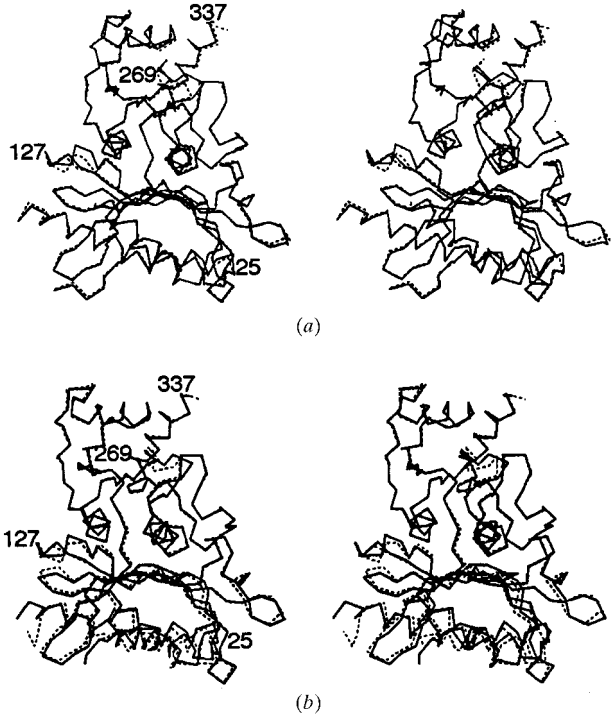

Figure 3
Least-squares superposition (*a*) of the rabbit liver monomer (unbroken line) and the C1 monomer of the pig kidney R-state Fru-6-P complex (PDB code 5FBP; broken line) and (*b*) of the rabbit liver monomer (unbroken line) and the pig kidney T-state AMP complex (4FBP; broken line). The least-squares fitting for (*b*) involved atoms in domain 2 (the catalytic domain) only.

Table 4
Secondary-structure elements in rabbit liver Fru-1,6-Pase.

Secondary element	Residue range
H1	Met13–Ala24
H2	Glu29–Val48
H3	Leu73–Ser87
B1	Thr91–Ser96
B2	Ile103–Ile104
B3	Arg110–Asp121
H4	Asn125–Cys128
B4	Ile132–Arg140
H5	Thr149–Ala152
H5a	Gly156–Asn158
B5	Ala161–Tyr167
B6	Thr171–Gly177
B7	Gly180–Asp187
B8	Glu192–Asp197
B9	Ile208–Ser210
H5b	Glu213–Asp218
H6	Pro221–Lys231
B10	Gly241–Ala242
H7	Met248–Tyr258
B11	Ile261–Tyr264
H8	Cys281–Ala291
B12	Met294–Thr296
H8a	Ile302–Asp304
B13	Val316–Gly319
H9	Pro321–Lys332

In contrast, when the monomers, dimers and tetramers of rabbit liver Fru-1,6-Pase were superimposed with the T-state pig kidney structure, the corresponding r.m.s. deviations were significantly higher (Table 5), confirming that the rabbit liver structure is in the R form. The r.m.s. deviations for monomer-to-monomer comparison between the rabbit liver subunit and T-state pig kidney monomers were around 1.1 Å; the dimers superimposed with similar r.m.s. deviations (1.2 Å). Superposition of two tetramers, however, resulted in a much larger overall deviation (3.2 Å). These numbers are consistent with the observations that, although the R→T transition in the pig kidney enzyme involves a 17° rotation between the C1C2 and C3C4 dimers, there is only a small (3.4°) rotation between two monomers comprising a dimer (Liang *et al.*, 1993). Interestingly, when domain 2 of the R-state rabbit liver protein was superimposed by least-squares onto domain 2 of the T-state pig kidney enzyme, the r.m.s. deviation was about 0.7 Å, a value similar to the r.m.s. deviations between the R-state monomers. This is consistent with the observation that the AMP-induced R→T allosteric transition in the pig kidney enzyme does not cause any appreciable structural change within the catalytic domain. However, superposition of domain 1 alone results in a larger deviation because of rearrangement within domain 1 during the R→T transition (Liang *et al.*, 1993; Zhang *et al.*, 1994).

3.3. Metal-binding site

As previously observed in pig kidney enzyme complexes involving Mg^{2+} (Ke, Zhang *et al.*, 1990; Zhang *et al.*, 1993), the

Table 5
R.m.s. deviations (Å) for Cα atoms in rabbit liver Fru-1,6-Pase superimposed by least squares on pig kidney R-state (5FPB) and T-state (4FBP) enzymes.

		Pig kidney					
		R form (5FBP; dimer in asymmetric unit)			T form (4FBP; tetramer in asymmetric unit)		
		Monomer(s)	Dimer	Tetramer	Monomer(s)	Dimer(s)	Tetramer
Rabbit liver R form (monomer in asymmetric unit)	Monomer	C1: 0.69	—	—	C1: 1.07	—	—
		C2: 0.67	—	—	C2: 1.10	—	—
		—	—	—	C3: 1.00	—	—
		—	—	—	C4: 1.09	—	—
	Dimer	—	C1C2: 0.71	—	—	C1C2: 1.21	—
		—	—	—	—	C3C4: 1.18	
	Tetramer	—	—	0.80	—	—	3.20
	Monomer domain 1	0.53	—	—	1.27	—	—
	Monomer domain 2	0.86	—	—	0.66	—	—

Mg^{2+} cation lies in a pocket formed by five negatively charged residues (Glu97, Glu98, Asp118, Asp21 and Glu280). As illustrated in Fig. 4, the Mg^{2+} is coordinated by the carboxylate side chains of four of these residues. Four of the metal ligands are the same as those constituting the so-called metal site 1 in the AhG-1,6-P_2 and AhM-1,6-P_2 ternary complexes of the pig kidney enzyme (Zhang *et al.*, 1993), but the fifth ligand (Glu97 OE1) is replaced by the 1-phosphate oxygen O11 in the substrate-analog complexes. Mn^{2+} and Zn^{2+} ions at site 1 do not coordinate atom Asp121 OD1 (Zhang *et al.*, 1993). The metal–oxygen distances are all in the 2.30–2.45 Å range, and it is significant that these distances were not restrained to any specific length during the refinement. The average metal–oxygen distance of 2.37 Å is somewhat shorter than the average Mg^{2+}–oxygen distances (2.5–2.6 Å) observed in the pig kidney R-form complexes (PDB codes 1FBC and 1FBF; Zhang *et al.*, 1993). The coordination geometry could be described as a distorted tetrahedron having an additional ligand from Glu97 or as a distorted octahedron in which the sixth ligand from the bottom (as viewed in Fig. 4) is missing. There are a few water molecules in the vicinity of the missing sixth ligand, and the closest such O atom is at a distance of 3.71 Å from the metal ion.

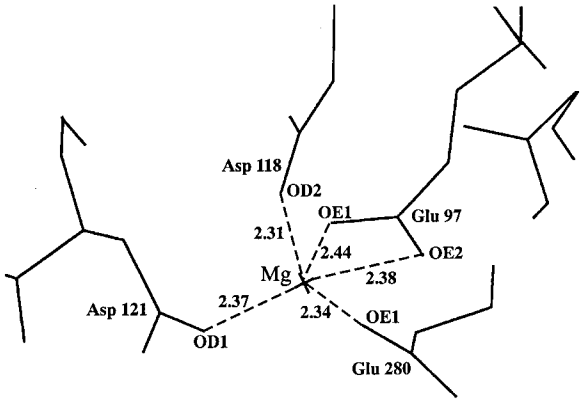

Figure 4
The cationic (Mg^{2+}) binding site in rabbit liver Fru-1,6-Pase. Coordination distances are in Å.

3.4. Sulfate binding

A sulfate ion is located (Fig. 5) at the position occupied by the 6-phosphate moiety in complexes of the pig kidney enzyme with product (Ke, Zhang *et al.*, 1990), with the competitive inhibitor Fru-2,6-P_2 (Liang *et al.*, 1992) and with substrate or substrate analogs (Zhang *et al.*, 1993). As illustrated in Fig. 6, this sulfate is coordinated by hydrogen bonds from the proton-donating side chains of Asn212, Tyr215, Tyr244 and Tyr264 as well as by salt-bridging interactions with the side chain of Arg243 from an adjacent crystallographically related subunit. In addition, several well ordered water molecules have been located in the vicinity of this sulfate ion, and some of these waters (*i.e.* W84 and W86) are within hydrogen-bonding distance of sulfate O atoms. The five sulfate-binding residues, along with Lys274, bind to the

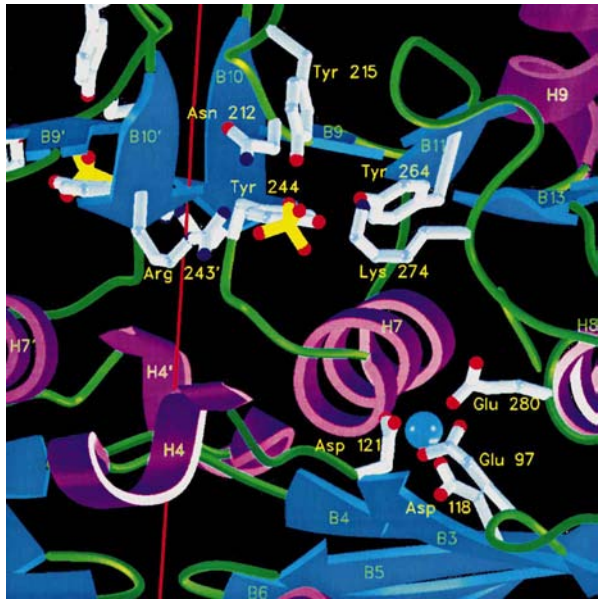

Figure 5
Two crystallographically related sulfate ions bound 20.8 Å apart at catalytic sites near the C1C2 dimer interface. The red line indicates the position of the crystallographic twofold axis; prime labels indicate a symmetry-related subunit. Atomic color codes are white (C), blue (N), red (O), yellow (S) and cyan (Mg). The figure was drawn using *SETOR*.

6-phosphate group in the pig kidney complexes. In this rabbit liver structure, the N atom of the Lys274 side chain is 3.68 Å from the closest sulfate O atom (see Fig. 5). All six phosphate-coordinating residues are strictly conserved in the mammalian primary structures (Liang *et al.*, 1992).

A second sulfate ion is located at a position corresponding to the allosteric site of pig kidney AMP complexes (Ke, Zhang *et al.*, 1990; Ke, Liang *et al.*, 1991; Xue *et al.*, 1994; Villeret, Huang, Zhang & Lipscomb, 1995). As illustrated in Fig. 7, the O atoms of this sulfate form five hydrogen-bonding contacts with the main-chain amides of residues Thr27, Gly 28, Glu29 and Met30, as well as three additional contacts with the side chains of Thr27, Lys112 and Tyr113. The backbone N atom of Gly28 forms a bifurcated hydrogen bond with two of the sulfate O atoms. These interactions of the sulfate ion with the rabbit liver protein are very similar to those of the phosphate moiety of AMP as observed in the complexes of the pig kidney enzyme.

3.5. Binding of β-methyl α-D-fructose-1,6-bisphosphate (β-methyl-Fru-1,6-P_2) at the catalytic site

A molecule of the non-hydrolyzable substrate analog β-methyl-Fru-1,6-P_2 was modeled into the 4 Å difference electron density at the catalytic cleft of domain 2. On account of the low resolution of the data for the substrate-analog complex, no attempt was made to refine this structure. Two of the three largest peaks in the difference map were used to position the β-methyl-Fru-1,6-P_2 molecule, as shown in Fig. 8. In this model, the largest of the three difference densities coincides with the furanose ring; the other two densities are near the 6-phosphate and the Mg^{2+} ion. However, the density for Mg^{2+} does not superimpose on the Mg^{2+} position obtained from the refinement of the structure in the absence of the substrate analog. This density is shifted by about 1 Å. Although movements of protein atoms in the catalytic cleft often accompany complexation, the overall orientation and position of the substrate analog in the cleft are consistent with refined models of Fru-6-P and Fru-2,6-P_2 in pig kidney complexes (Ke, Zhang *et al.*, 1991; Liang *et al.*, 1992). The interactions of the Mg^{2+} ion and the 6-phosphate moiety with protein atoms are similar to the interactions already described for Mg^{2+} ion (Fig. 4) and for sulfate (Fig. 6) in the absence of the substrate analog. No strong electron density for the 1-phosphate could be located. Modeling suggests that this phosphate group could interact with the Ser124 hydroxyl and the Lys274 amino groups.

4. Discussion

The crystal structure determination reported here, along with the report of the primary structure (Kaiser *et al.*, 1996), resolve the conflicts between previous rabbit liver Fru-1,6-Pase sequence data and the sequences of related species. The rabbit liver enzyme has now been shown to be a normal member of this enzyme family, with its overall primary, secondary, tertiary and quaternary structures similar to those of the extensively studied pig kidney enzyme. All of the residues critical for metal, substrate and competitive-inhibitor binding are present, including residues Asp121, Asn125 and Glu280, which were missing in the original rabbit liver sequence data. The 36 amino-acid differences between the rabbit liver and pig kidney enzymes, including 22 modifications in α-helical or β-sheet regions, result in only minor conformational changes. Instead, the largest differences are observed in loops with high thermal motion. The rabbit liver enzyme has three additional short 3_{10}-helical regions.

The presence of an apparent single Mg^{2+} cation in the rabbit liver structure is noteworthy. This ion refines well as a fully occupied Mg^{2+} site, but it refines poorly when modeled as Mn^{2+} or as NH_4^+. It displays a coordination pattern typical of Mg^{2+} but not of Mn^{2+} or Zn^{2+} (Zhang *et al.*, 1993). No Mg^{2+}

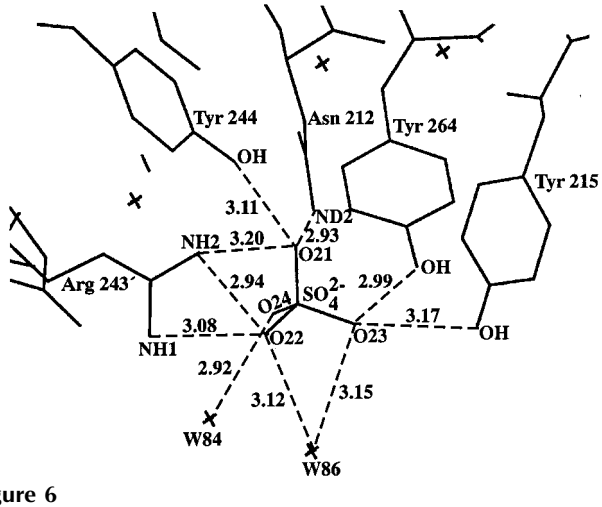

Figure 6
Coordination of the sulfate ion at the site occupied by the 6-phosphate group of pig kidney enzyme complexes with product, competitive inhibitor, substrate and substrate analogs. Hydrogen-bond distances ≤3.2 Å are indicated.

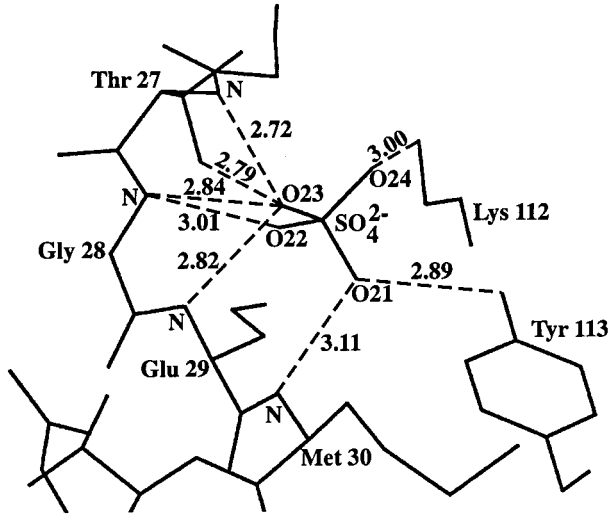

Figure 7
Coordination of the sulfate ion at the site occupied by the phosphate moiety of AMP in the pig kidney enzyme complexes. Hydrogen-bond distances ≤3.2 Å are indicated.

was added during the isolation or crystallization procedures, both of which involved extensive dialysis and other procedures designed to remove salt. This suggests that Mg^{2+} is intrinsic to the rabbit liver enzyme. It was shown by binding studies (Benkovic *et al.*, 1978) that there are two divalent metal binding sites per subunit, a high-affinity structural site (M1) and a low-affinity catalytic site (M2). However, recent kinetic (Liu & Fromm, 1990) and crystallographic data (Zhang *et al.*, 1993) both indicate that, although two Mn^{2+} and Zn^{2+} cations bind per subunit, Mg^{2+} binds only to the M1 site. The M1 site is occupied in this rabbit liver structure.

Two sulfate ions, the presence of which appears to be necessary for the growth of diffraction-quality crystals, are bound to the sites occupied by the 6-phosphate moiety of the substrate and the phosphate group of the allosteric inhibitor AMP in pig kidney Fru-1,6-Pase structures. Least-squares fitting experiments with pig kidney R- and T-state models clearly demonstrate that this rabbit liver enzyme structure has an active R conformation, and the sulfate bound to the allosteric site does not appear to cause any structural rearrangement. The hydrogen bonds from the active-site sulfate to residues Asn212, Tyr215, Tyr244 and Tyr264 of one monomer, coupled with simultaneous interaction of this sulfate with Arg243 of another monomer, may provide the conformational stability necessary for diffraction-quality crystals.

Although mammalian Fru-1,6-Pases are all regulated by AMP, the affinity of the enzyme for this allosteric inhibitor varies widely, and even greater variation is observed in enzymes from distantly related species where AMP has little or no effect. For example, K_i values for AMP range from below 1 μM for the rabbit skeletal muscle enzyme (Black *et al.*, 1972), through 10–20 μM for the liver and kidney enzymes (Colombo & Marcus, 1973) and 80–200 μM for the yeast enzymes (Marcus *et al.*, 1988), to no AMP inhibition for chloroplast (Preiss *et al.*, 1967; Buchanan *et al.*, 1971) and bumblebee flight muscle (Newsholme *et al.*, 1972) enzymes. The residues which interact with divalent cations, substrate and the 2-phosphate group of Fru-2,6-P_2 are strongly conserved but, as might be expected from the variation in AMP sensitivity, conservation of the AMP-binding residues (17–31, 112–113, 140, 160 and 177) is low (Ke, Liang *et al.*, 1991). Interestingly, the longest string of amino-acid differences between the rabbit liver and pig kidney enzymes occurs in the tripeptide at positions 177–179 where the Met–Val–Asn sequence in the pig kidney protein is replaced by Gly–Gly–Ser in the rabbit liver form. The purine base of AMP bound at the allosteric site of the pig kidney enzyme makes a van der Waals contact with the Met177 side chain (Ke, Liang *et al.*, 1991). Although no significant deviation of backbone atoms in this region was observed when the two structures were superimposed, the change of Met177 and Val178 to glycine residues increases the space available in the vicinity of the purine base and reduces the hydrophobic character of the AMP-binding pocket of the rabbit liver structure. Further evidence that the Met177 interaction is not critical for AMP inhibition comes from the unchanged apparent K_i for AMP in the Met177→Ala mutant of the human liver enzyme (Gidh-Jain *et al.*, 1994).

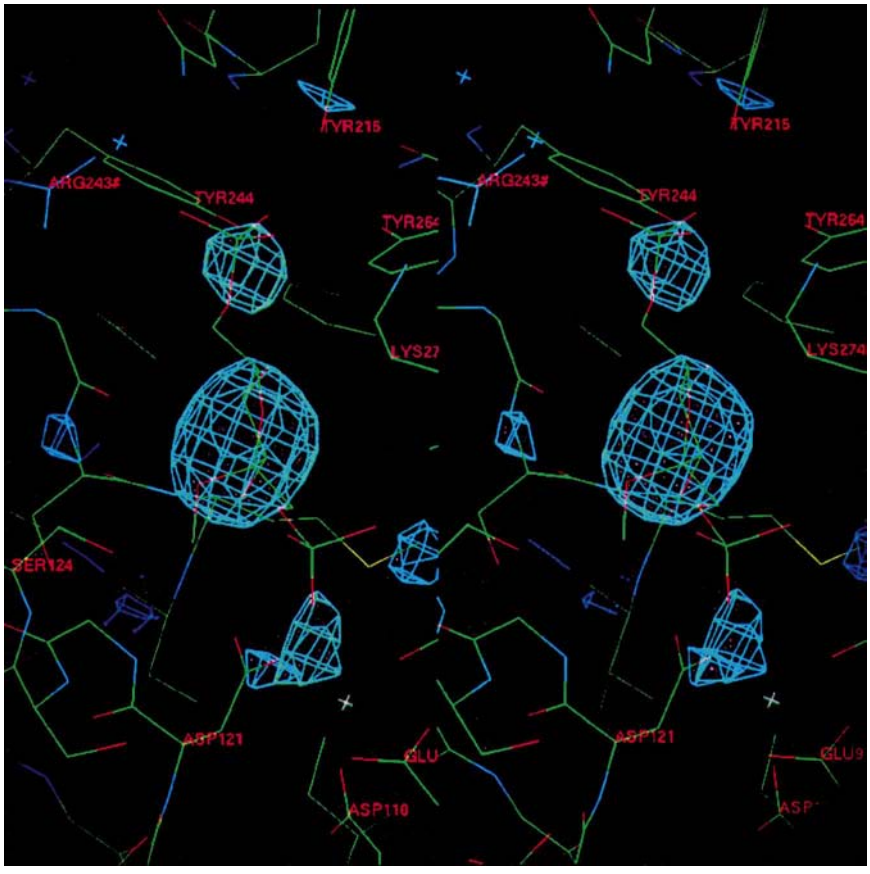

Figure 8
Stereoview showing the three largest peaks, contoured at 4σ, in the difference electron density for the β-methyl-Fru-1,6-P_2 complex.

The authors are indebted to Dr Alexander McPherson who initiated the project and supplied the first crystals. We are also grateful to Dr Zdzislaw Wawrzak for help with the computations and to Mary and Edwin Westbrook, as well as the staff of Dr Nguyen Xuong's laboratory, for assistance with data collection. This research was supported in part by grants from the James H. Cummings Foundation, the USA National Institutes of Health (AM25192) and the Swedish Medical Research Council (13X-3532).

References

Benkovic, P. A., Caperelli, C. A., deMaine, M. M. & Benkovic, S. J. (1978). *Proc. Natl Acad. Sci. USA*, **75**, 2185–2189.
Benkovic, S. J. & deMaine, M. M. (1982). *Adv. Enzymol. Relat. Areas Mol. Biol.* **53**, 45–82.

Black, W. J., Van Tol, A., Fernando, J. & Horecker, B. L. (1972). *Arch. Biochem. Biophys.* **51**, 576–590.
Botelho, L. H., El-Dorry, H. A., Crivellaro, O., Chu, D. K., Pontremoli, S. & Horecker, B. L. (1977). *Arch. Biochem. Biophys.* **184**, 535–545.
Brünger, A. T. (1992). *X-PLOR Manual Version 3.1.* New Haven: Yale University Press.
Buchanan, B. B., Schurmann, P. & Kalberer, P. P. (1971). *J. Biol. Chem.* **246**, 5952–5959.
Colombo, G. & Marcus, F. (1973). *J. Biol. Chem.* **248**, 4923–4925.
El-Maghrabi, M. R., Gidh-Jain, M., Austin, L. A. R. & Pilkis, S. J. (1993). *J. Biol. Chem.* **268**, 9466–9472.
El-Maghrabi, M. R., Pilkis, J., Marker, A., Colosia, A. D., D'Angelo, G., Fraser, B. A. & Pilkis, S. F. (1988). *Proc. Natl Acad. Sci. USA*, **85**, 8430–8434.
Engh, R. A. & Huber, R. (1991). *Acta Cryst.* A**47**, 392–400.
Evans, S. V. (1993). *J. Mol. Graph.* **11**, 134–138.
Fisher, W. K. & Thompson, E. O. P. (1983). *Aust. J. Biol. Sci.* **36**, 235–250.
Furey, W. & Swaminathan, S. (1990). Annu. Meet. Am. Crystallogr. Assoc., p. 73, Abstract PA33.
Gidh-Jain, M., Zhang, Y., van Poelje, P. D., Liang, J.-Y., Huang, S., Kim, J., Elliott, J. T., Erion, M. D., Pilkis, S. J., El-Maghrabi, M. R. & Lipscomb, W. N. (1994). *J. Biol. Chem.* **269**, 27732–27738.
Gomori, G. (1943). *J. Biol. Chem.* **148**, 139–149.
Harrsch, P. B., Kim, Y., Fox, J. L. & Marcus, F. (1985). *Biochem. Biophys. Res. Commun.* **133**, 520–526.
Horecker, B. L., MacGregor, J. S., Singh, V. N., Tsolas, O., Sun, S. C., Crivellaro, O. & Pontremoli, S. (1980). *FEBS Enzyme Regulation and Mechanism of Action*, edited by P. Mildner & B. Reis, Vol. 60, pp. 3–14. New York: Pergamon Press.
Hubert, E., Villanueva, J., Gonzalez, A. M. & Marcus, F. (1970). *Arch. Biochem. Biophys.* **138**, 590–597.
Kaiser, R., Olsson, H., Erman, M., Weeks, C. M., Hjelmqvist, L., Ghosh, D. & Jörnvall, H. (1996). *FEBS Lett.* **389**, 249–252.
Ke, H., Liang, J.-Y., Zhang, Y. & Lipscomb, W. N. (1991). *Biochemistry*, **30**, 4412–4420.
Ke, H., Thorpe, C. M., Seaton, B. A., Lipscomb, W. N. & Marcus, F. (1990). *J. Mol. Biol.* **212**, 513–539.
Ke, H., Thorpe, C. M., Seaton, B. A., Marcus, F. & Lipscomb, W. N. (1989). *Proc. Natl Acad. Sci. USA*, **86**, 1475–1479.
Ke, H., Zhang, Y., Liang, J.-Y. & Lipscomb, W. N. (1991). *Proc. Natl Acad. Sci. USA*, **88**, 2989–2993.
Ke, H., Zhang, Y. & Lipscomb, W. N. (1990). *Proc. Natl Acad. Sci. USA*, **87**, 5243–5247.
Laskowski, R. A., MacArthur, M. W., Moss, D. S. & Thornton, J. M. (1993). *J. Appl. Cryst.* **26**, 283–291.
Liang, J.-Y., Huang, S., Zhang, Y., Ke, H. & Lipscomb, W. N. (1992). *Proc. Natl Acad. Sci. USA*, **89**, 2404–2408.
Liang, J.-Y., Zhang, Y., Huang, S. & Lipscomb, W. N. (1993). *Proc. Natl Acad. Sci. USA*, **90**, 2132–2136.
Liu, F. & Fromm, H. J. (1990). *J. Biol. Chem.* **265**, 7401–7406.
Lu, G., Stec, B., Giroux, E. L. & Kantrowitz, E. R. (1996). *Protein Sci.* **5**, 2333–2342.
Luzzati, V. (1952). *Acta Cryst.* **5**, 802–810.
MacGregor, J. S., Hannappel, E., Xu, G.-J., Pontremoli, S. & Horecker, B. L. (1982). *Arch. Biochem. Biophys.* **217**, 652–664.
McPherson, A., Burkey, D. & Stankiewicz, P. (1977). *J. Biol. Chem.* **252**, 7031–7034.
Marcus, F. (1981). *The Regulation of Carbohydrate Formation and Utilization in Mammals*, edited by C. M. Veneziale, pp. 269–290. Baltimore: University Park Press.
Marcus, F., Edelstein, I., Reardon, I. & Heinrikson, R. L. (1982). *Proc. Natl Acad. Sci. USA*, **79**, 7161–7165.
Marcus, F., Rittenhouse, J., Moberly, L., Edelstein, I., Hiller, E. & Rogers, D. T. (1988). *J. Biol. Chem.* **263**, 6058–6062.
Newsholme, E. A., Crabtree, B., Higgins, S. J., Thornton, S. D. & Start, C. (1972). *Biochem. J.* **128**, 89–97.
Pontremoli, S., Accorsi, A., Melloni, E., Schiavo, E., DeFlora, A. & Horecker, B. L. (1974). *Arch. Biochem. Biophys.* **164**, 716–721.
Pontremoli, S., Melloni, E., Balestrero, F., Franzi, A. T., DeFlora, A. & Horecker, B. L. (1973). *Proc. Natl Acad. Sci. USA*, **70**, 303–305.
Preiss, J., Biggs, M. L. & Greenberg, E. (1967). *J. Biol. Chem.* **242**, 2292–2294.
Sack, J. S. (1988). *J. Mol. Graph.* **6**, 224–225.
Soloway, B. & McPherson, A. (1978). *J. Biol. Chem.* **253**, 2461–2462.
Stec, B., Abraham, R., Giroux, E. L. & Kantrowitz, E. R. (1996). *Protein Sci.* **5**, 1541–1553.
Suda, H., Xu, G.-J., Kutny, R. M., Natalini, P., Pontremoli, S. & Horecker, B. L. (1982). *Arch. Biochem. Biophys.* **217**, 10–14.
Taketa, K. & Pogell, B. M. (1965). *J. Biol. Chem.* **240**, 651–662.
Tashima, Y., Tholey, G., Drummond, G., Bertrand, H., Rosenberg, J. S. & Horecker, B. L. (1972). *Arch. Biochem. Biophys.* **149**, 118–126.
Tejwani, G. A. (1983). *Adv. Enzymol. Relat. Areas Mol. Biol.* **54**, 121–194.
Terwilliger, T. C. & Eisenberg, D. (1983). *Acta Cryst.* A**39**, 813–817.
Traniello, S., Melloni, E., Pontremoli, S., Sia, C. L. & Horecker, B. L. (1972). *Arch. Biochem. Biophys.* **149**, 222–231.
Traniello, S., Pontremoli, S., Tashima, Y. & Horecker, B. L. (1971). *Arch. Biochem. Biophys.* **146**, 161–166.
Ulm, E. H., Pogell, B. M., deMaine, M. M., Libby, C. B. & Benkovic, S. J. (1975). *Methods Enzymol.* **42**, 369–374.
Van Schaftingen, E. (1987). *Adv. Enzymol. Relat. Areas Mol. Biol.* **59**, 315–395.
Van Schaftingen, E. & Hers, H.-G. (1980). *Biochem. Biophys. Res. Commun.* **96**, 1524–1531.
Van Schaftingen, E. & Hers, H.-G. (1981). *Proc. Natl Acad. Sci. USA*, **78**, 2861–2863.
Villeret, V., Huang, S., Fromm, H. J. & Lipscomb, W. N. (1995). *Proc. Natl Acad. Sci. USA*, **92**, 8916–8920.
Villeret, V., Huang, S., Zhang, Y. & Lipscomb, W. N. (1995). *Biochemistry*, **34**, 4307–4315.
Villeret, V., Huang, S., Zhang, Y., Xue, Y. & Lipscomb, W. N. (1995). *Biochemistry*, **34**, 4299–4306.
Weeks, C. M., Erman, M. & Ghosh D. (1988). Annu. Meet. Am. Crystallogr. Assoc., Abstract PD7.
Williams, M. K. & Kantrowitz, E. R. (1992). *Proc. Natl Acad. Sci. USA*, **89**, 3080–3082.
Xu, G.-J., Natalini, P., Suda, H., Tsolas, O., Dzugaj, A., Sun, S. C., Pontremoli, S. & Horecker, B. L. (1982). *Arch. Biochem. Biophys.* **214**, 688–694.
Xue, Y., Huang, S., Liang, J.-Y., Zhang, Y. & Lipscomb, W. N. (1994). *Proc. Natl Acad. Sci. USA*, **91**, 12482–12486.
Zhang, Y., Liang, J.-Y., Huang, S., Ke, H. & Lipscomb, W. N. (1993). *Biochemistry*, **32**, 1844–1857.
Zhang, Y., Liang, J.-Y., Huang, S. & Lipscomb, W. N. (1994). *J. Mol. Biol.* **244**, 609–624.